Synthetic seismicity
for the San Andreas fault

Saskia D.B. Goes and Steven N. Ward
Institute of Tectonics and Richter Seismological Laboratory, University of California,
Santa Cruz, CA, U.S.A.

Abstract

Because historical catalogs generally span only a few repetition intervals of major earthquakes, they do not provide much constraint on how regularly earthquakes recur. In order to obtain better recurrence statistics and long-term probability estimates for events $M \geq 6$ on the San Andreas fault, we apply a seismicity model to this fault. The model is based on the concept of fault segmentation and the physics of static dislocations which allow for stress transfer between segments. Constraints are provided by geological and seismological observations of segment lengths, characteristic magnitudes and long-term slip rates. Segment parameters slightly modified from the Working Group on California Earthquake Probabilities allow us to reproduce observed seismicity over four orders of magnitude. The model yields quite irregular earthquake recurrence patterns. Only the largest events ($M \geq 7.5$) are quasi-periodic; small events cluster. Both the average recurrence time and the aperiodicity are also a function of position along the fault. The model results are consistent with paleoseismic data for the San Andreas fault as well as a global set of historical and paleoseismic recurrence data. Thus irregular earthquake recurrence resulting from segment interaction is consistent with a large range of observations.

Key words *seismicity – model – San Andreas fault – seismic hazard – fault segments*

1. Introduction

Because most earthquake catalogs span no more than a few recurrences, they provide limited information on earthquake recurrence behavior. As an alternative way to study what factors control the occurrence of earthquakes, various seismicity models have been developed over the years. Studies by for example Ben-Zion and Rice (1993), Chen and Knopoff (1987), Rundle (1988a) and Harris and Day (1993) focus on the complex physics of faulting including dynamic rupture, rate and state dependent friction laws and seismic radiation. Other studies (*e.g.* Stuart 1986; Rundle 1988b; Ward 1991, 1992a,b) have instead constrained models by earthquake data, as a tool in estimating seismic hazard. This is the approach

taken in this study. To use a model for hazard analyses, a balance has to be found between including a realistic physical representation and keeping the model simple enough to contrain with the limited observations. Although based on simplified physics, our synthetic catalog is consistent with a large range of earthquake data, from geologic slip rates and segment boundaries to seismicity levels observed along the fault and recurrence records retrieved by paleoseismic work.

Most previous seismic hazard analyses have been based on models more simplified than ours. The time- or slip-predictable models proposed by Shimazaki and Nakata (1980) derive hazard estimates solely from time since or slip during the previous event. The seismic gap model as it was applied in several hazard analyses (*e.g.* McCann *et al.*, 1979; Nishenko, 1985; Working Group of California Earthquake Probabilities (WGCEP) 1988, 1990) assumes quasi-periodic earthquake recurrence which
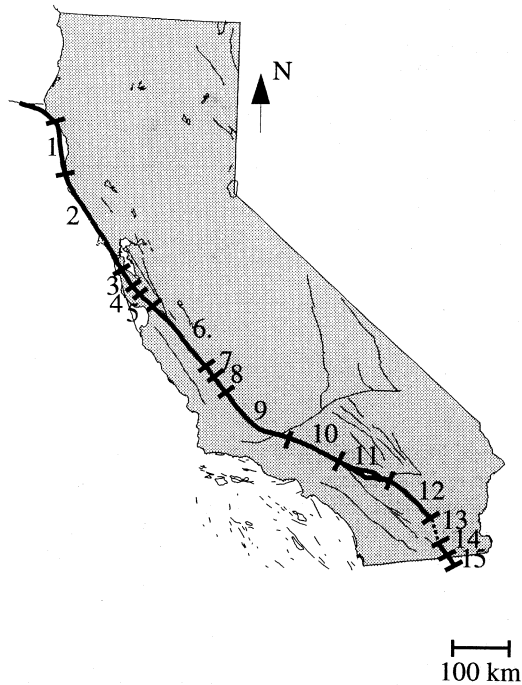
H——H
100 km

Fig. 1. Map of California with its major faults. The San Andreas and Imperial Valley faults (segment 14-15) are shown in bold. The numbered segments are used as input for our synthetic seismicity calculations. Segment names and parameters are in table I.

allows for probability estimates based on average recurrence interval and time since the last event. Our seismicity model produces stress and slip histories and includes a reasonable approximation of the effect of segment interaction.

Several observations indicate that segment interaction may be important in determining earthquake recurrence behavior. For example the Parkfield event in 1934 occurred 10 years earlier than would be expected based on the average recurrence time of 22 years for this segment (Bakun and Lindh, 1985). This short recurrence interval has been attributed to premature triggering of the event. Similarly, segments that have been observed to fail independently, sometimes fail together with neighboring segments in much larger events (*e.g.*

Kanamori and McNally, 1982; Nishenko and Singh, 1987; Thatcher, 1990). Another example is the migration of foci that has been observed for many regions around the world (*e.g.* King and Ma, 1988; Nishenko, 1985). These observations point to an important role of stress transfer between fault segments.

This paper describes the application of our synthetic seismicity model to the San Andreas fault (see also Ward and Goes, 1993). The San Andreas is the main fault delineating the plate boundary between North American and Pacific plates (fig. 1). Although a considerable part of the plate motion is taken up along smaller faults both in the San Andreas fault system as well as in the Transverse Ranges, the Eastern Mojave Shear Zone and the Basin and Range province, the San Andreas is responsible for producing the largest earthquakes which may affect densely populated areas. Besides the importance of seismic hazard estimates for the San Andreas fault, the large amount of research (*e.g.* Sykes and Nishenko, 1984; Wesnousky, 1986; WGCEP, 1988, 1990) that has gone into characterizing seismicity of this fault, provides a good data base to constrain our models.

2. Model

The modeling procedure we used was previously applied to the Middle American Trench (Ward, 1991, 1992a,b). It can be summarized as a segment interaction model where the stress transfer between segments is prescribed by static dislocation theory. We consider stress along the fault only. The model requires a small set of input parameters, most importantly a set of segments (table I). The fault segments are each characterized by a length, strength, and long term slip rate (which controls the stress accumulation rate). The length plus (static) strength of a segment define what the characteristic magnitude is of an earthquake which breaks the entire segment, independent of its neighbors. Other input parameters are the width of the seismogenic zone (W) and the rigidity (μ) (table II). Further we include a stress drop-slip relation to prevent escalation of

1496

Table I. Segment parameters, slightly modified from WGCEP (1988, 1990) segments to fit the observed seismicity (fig. 6).

	Segment name	Length (km)	M_{char}	Slip rate (mm/yr)
1	Mendocino	100	7.0	18
2	North Coast	240	7.6	18
3	Mid Peninsula	41	7.0	18
4	N. Santa Cruz Mtns.	20	6.5	18
5	S. Santa Cruz Mtns.	39	6.9	18
6	Central Creeping Zone	140		36
7	Parkfield	30	6.3	36
8	Cholame	55	7.0	36
9	Carrizo	145	7.7	36
10	Mojave	100	7.45	36
11	San Bernadino Mtns.	100	7.25	24
12	Coachella Valley	100	7.35	24
13	Brawley Seismic Zone	50		30
14	N. Imperial Valley	30	6.5	30
15	S. Imperial Valley	30	6.6	30

Table II. Preferred values of model parameters.

Parameter	Value
μ	$3 \cdot 10^{10}$ N/m^2
W	11 km
V_c	18 mm/yr
ΔV_c	3 mm/yr
T_m	10 yr

ruptures. This relation requires three additional parameters, a memory time (T_m), a reference velocity (V_r) and variation around the reference velocity (ΔV_r) (table II).

The model uses static dislocations to calculate stress and slip along the fault in an iterative manner (Ward, 1991). It is made time de-pendent by adding an increment of stress in each time step. If stress reaches the strength anywhere on the fault, that part breaks in a «synthetic» earthquake. There are two modes of failure, the first one being in small earthquakes if only part of a segment breaks. In this case stress drops back down to the (static) strength. Repeated small earthquakes may eventually «erode» the whole segment, by stressing the entire segment to its strength level. In that case the whole segment fails in a large event, dropping the stress level to a lower dynamic strength level. A strain hardening condition (Ward, 1991) keeps segments from failing repeatedly in large events. This relation controls the dynamic strength and essentially lowers the stress drop if the recent rate of slip was large compared to the reference slip rate $V_r \pm \Delta V_r$. After a long time without slip, relative to the memory time T_m, the stress drop re-
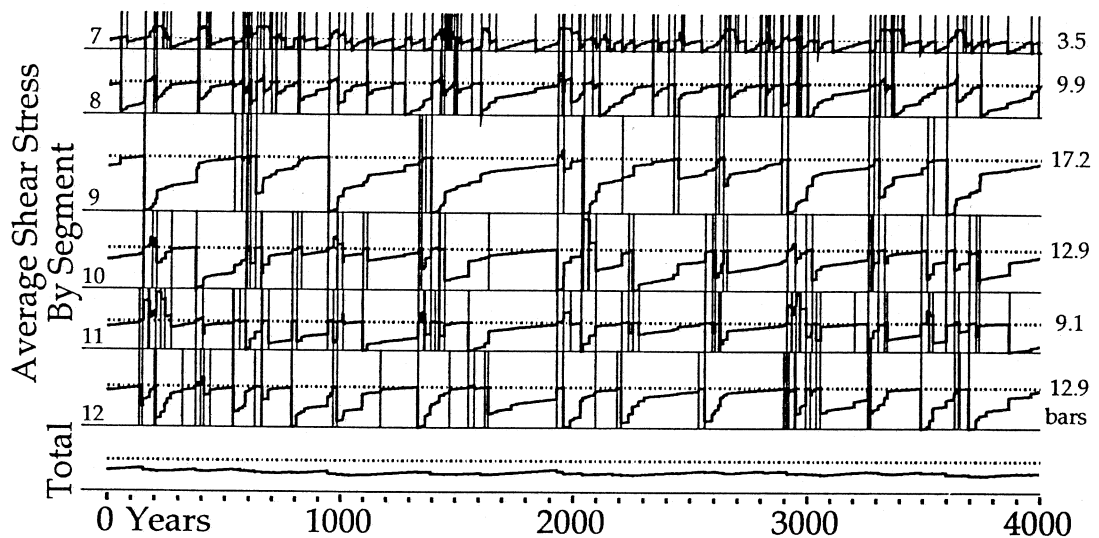
Fig. 2. Segment averaged stress for Parkfield (# 7) to Coachella Valley (# 12) segments. Dashed and solid horizontal lines represent the static strength and zero stress levels for each segment. Vertical lines represent segment-breaking earthquakes of magnitude 6 or greater. Significant stress transfer between segments results in much more irregular stress build-up than would be expected from tectonic loading alone. Note that despite the highly variable stress states of the individual segments, the mean stress over the entire fault (bottom) is nearly constant.

turns to the value of the static strength. This is necessary to keep seismic moment from being released in unrealistic large pulses of clustered large events. The model produces general characteristics of earthquake behavior such as foreshocks, aftershocks, and migration of foci, as was shown by Ward (1991).

3. Output

The model generates a stress and slip history along the fault. In contrast to historical catalogs which generally comprise only a few recurrence intervals, the model can be run for as long as necessary to obtain a statistically significant number of repeats. We ran models of 100 000 years with 2 year time steps. This long synthetic catalog assures adequate sampling for reliable statistics, even for the largest events ($M \approx 8$). The two year time step is too

large to sufficiently model the smallest events ($M \leq 4$). However, the time step does not affect the recurrence of events larger than $M4$. In this study we focus on the largest events, $M \geq 6$, which contribute most to seismic hazard along the San Andreas fault.

3.1. Stress

The synthetic stress history (fig. 2) clearly shows the effect of segment interaction. In general, stress increases due to large scale plate motions. However, failure of nearby segments disrupts this regular stress build-up and introduces steps which advance the time until the next earthquake. These stress steps are similar to the two-dimensional static stress changes calculated by Harris and Simpson (1992) and Stein et al. (1992) for the recent Landers earthquake. If segment interaction is as strong as

modeled here, stress jumps resulting from failure of neighboring segments largely control when future events are going to occur.

3.2. *Slip*

The slip history (figs. 3 and 4) illustrates how the jagged stress profile results in earthquake patterns that are quite irregular. Figure 3 shows the cumulative slip for a representative 1000 year interval of the model. Each pillow corresponds to a slip event. The two blackened

areas (the Central Creeping and Brawley Seismic zone) behave aseismically, slipping easily without generating earthquakes. While characteristic earthquakes (repeating, segment-breaking events) occur (*e.g.* segment 9), much of the slip is taken up by non-characteristic events where segments fail in part or completely in conjunction with one or more of their neighbors. Another result of the interactive behavior is that segment boundaries are not strongly reflected in the seismicity. The slip accumulated along the fault varies. This variation is the result of changes in slip rate which reflect the
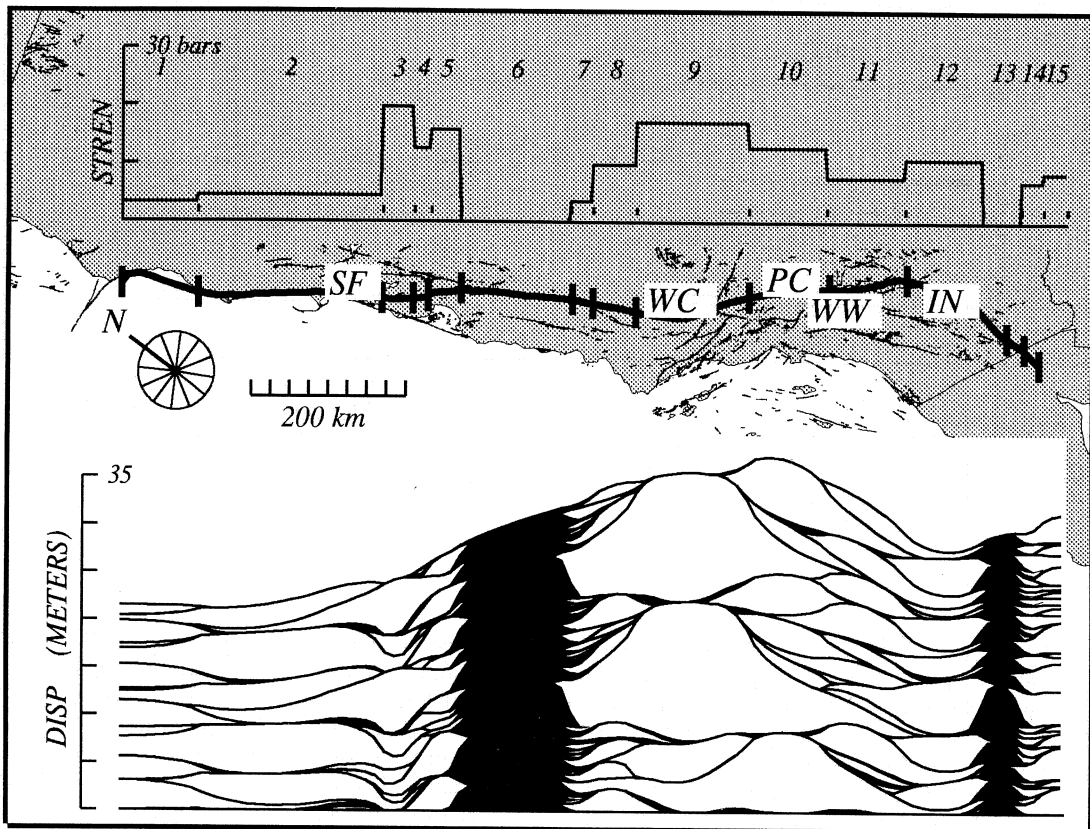

Fig. 3. Synthetic seismicity for the San Andreas fault. Cumulative slip for a typical 1000 year section of the model. Each pillow represents the slip in a large quake. The blackened areas in the Central Creeping section and the Brawley seismic zone are aseismic. Note the mixture of characteristic and non-characteristic events. On the map the strength profile of the segments used is shown.
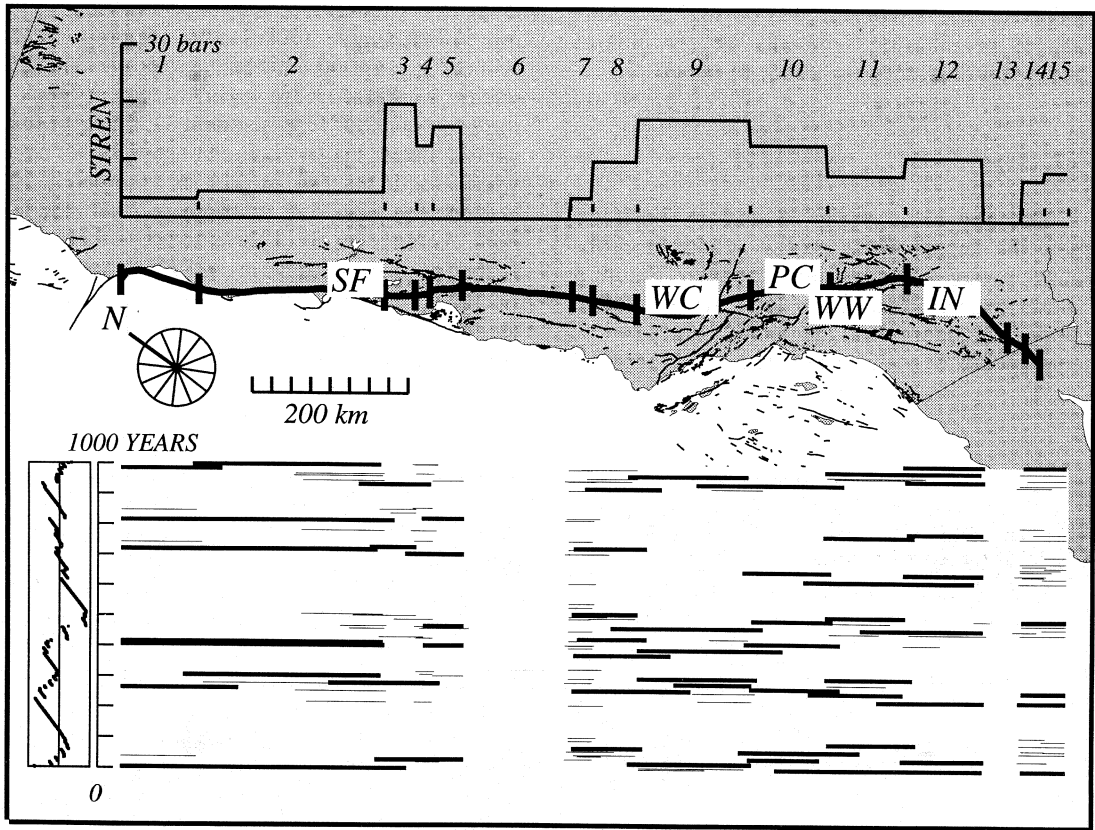
Fig. 4. Space-time diagram for the same time interval as shown in fig. 3. Lines show the extent of rupture for all events $M \geq 6$, bold lines showing events with magnitudes exceeding 7. The small box on the left depicts the moment release as it varies around the tectonic moment at each time step. The scale of the box is plus or minus the moment released by an $M8$ event.

fact that part of the large scale plate motions are taken up along faults parallel to the San Andreas, such as the Hayward-Rogers Creek-Maacama fault zone in the north and the San Jacinto fault in the south.

Figure 4 summarizes the seismicity from fig. 3 in a space-time diagram. Rupture zones for events larger than $M6$ are shown, thick lines mark events with magnitudes over 7. The small box on the left shows the variation of moment release as a function of time. The synthetic event history exhibits many of the characteristics of seismicity along the San Andreas fault, for example, large events similar to the historical 1906 and 1857 earthquakes. Small earthquakes occur regularly on only a few segments, such as the Southern Santa Cruz Mountains, Parkfield and the two Imperial Valley fault segments, consistent with the relative quiescence of most of the San Andreas observed in historical times. The Parkfield segment produces earthquakes on a regular basis but not as regularly as the six documented Parkfield events suggest (Bakun and Lindh, 1985).

4. Model constraints

The model was tailored to the San Andreas fault with a range of data. Segment positions and lengths were derived from geological (changes in slip rate, fault strike, stepovers) and seismological (rupture lengths of large earthquakes) observations. We relied on a segmentation drawn by the WGCEP (1988, 1990) which integrated much of the available San Andreas data. For each of their segments, the Working Group estimated a characteristic magnitude and a slip rate. Strain hardening parameters (table II) were based on the condition that moment release has to be a relatively smooth function of time. Moment release at any given time should not deviate from the expected average moment release more than the moment that is produced by a $M8$ earthquake (fig. 4).

The range of allowable segment parameter values was further constrained by the observed frequency versus magnitude distribution. Firstly, this distribution gives an estimate of the total moment release per year which bounds the slip rates and the width of the seismogenic zone (table III). Observed slip rates are 19 ± 4 mm/yr for the Northern San An-

dreas (WGCEP, 1990) and 30 ± 5 mm/yr for the Southern San Andreas (WGCEP, 1988). A seismogenic width of 10 km satisfies these constraints on slip rate (table III). Secondly, although there is no straightforward relation between the number and size of segments necessary to produce the observed magnitude frequency curve, we claim that the shape of the curve yields information on possible rupture scenarios and therefore segment sizes.

4.1. Seismicity distribution and characteristic earthquake behavior

Previous work has proposed that single segments produce «characteristic» earthquake distributions (Wesnousky et al., 1983; Schwartz and Coppersmith, 1984; Davison and Scholz, 1985). A characteristic distribution shows an excess of large events compared to the trend delineated by the numbers of small events, implying that for a single segment there is one particular size of event which releases the bulk of the moment. The segments in our model behave characteristically if they can fail mostly independent from their neighbors, as is illustrated by the magnitude-frequency curve for the Carrizo segment (# 9) (fig. 5). When a fault consists of several segments with different characteristic magnitudes, the shape of the magnitude-frequency curve is expected to reflect the bumps for the different possible characteristic events. Building on the characteristic earthquake concept, Wesnousky (1994) used geologic slip rates, fault lengths and different segment combinations to predict the shape of the magnitude-frequency curve and extrapolate to the largest expected event. However, if segment interaction plays a role, the relation between seismicity and segmentation is significantly more complex. Segment interaction increases the number of possible rupture scenarios, resulting in a larger variety in «characteristic» event sizes. An example of a magnitude-frequency curve which reflects segment interaction is shown in fig. 5 for the Parkfield segment (# 7), which besides generating its own $M6$ events, also fails in larger ruptures that involve one or more of its southern neighbors.

Table III. Constraints on width of the seismogenic zone (W) and average slip rates for the Northern San Andreas (NSA) and the Southern San Andreas (SSA, includes the Imperial Valley fault) from observed seismic moment rates ($M_{0,\mathrm{obs}}$) and geologic slip rates ($V_{c,\mathrm{obs}}$). A width of 10 km was used in the modeling.

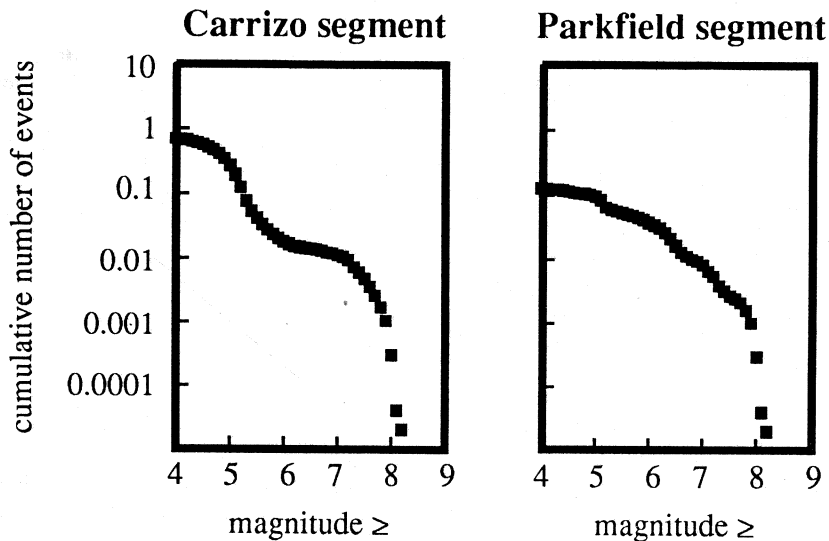|	NSA	SSA	W (km)
$M_{0,\mathrm{obs}}$ (Nm/yr)	$2.55 \cdot 10^{18}$	$6.05 \cdot 10^{18}$	
$V_{c,\mathrm{obs}}$ (mm/yr)	19 ± 5	30 ± 5	
$V_{c,\mathrm{calc}}$ (mm/yr)	19.3	34.2	10
	17.6	31.1	11
	16.1	28.5	12
	14.9	26.3	13

Fig. 5. Magnitude-frequency curves of individual model segments reflect the segment's own parameters as well as the extent to which segment failure is influenced by neighboring segments. The strong Carrizo segment shows characteristic behavior, producing mainly its own characteristic type earthquakes and aftershocks. The Parkfield segment produces a larger range of events as a result of its position as a small segment next to stronger neighbors.

4.2. Magnitude-frequency data

The magnitude-frequency data (fig. 6) used to constrain our San Andreas fault model were combined from the Berkeley and Caltech catalogs (events with $M < 6$ for 1932-1987 and 1932-1991 respectively) and a catalog for major earthquakes in California ($M \geq 6$, 1900-1989) compiled by Ellsworth (1990) to which the major events from the Landers sequence (April-June 1992) were added. For the periods indicated these three catalogs are probably complete. All events within a band of 40 km centered around the San Andreas fault were included. As an estimate of the uncertainty in the shape of the magnitude-frequency curve due to the shortness of the catalogs, we determined the variation in 200 year magnitude-frequency distributions from the model results (fig. 6 top). Two hundred years is about the length of the San Andreas catalog of large events.

The observed magnitude frequency distributions for the whole fault as well as for the San Andreas north of the creeping zone and south of the creeping zone (fig. 6) show a smooth trend with no clear preference for any characteristic size event. The variation in shape of the magnitude-frequency curve along the San Andreas fault (fig. 6) may be an expression of the different segment characteristics along the fault. The slightly modified WGCEP segments used in our model (table I) are able to reproduce this observed variation in seismicity quite well (fig. 6). However, other segmentations may be capable of reproducing the observed seismicity. Adding a few more segments with characteristic magnitudes around $M5.5$ may improve the fit of the corresponding part of the magnitude-frequency distribution. For lack of constraints for such segments, we focus on the larger events which are reproduced well by the model.

1502

5. Recurrence statistics

Because of the variability in both earthquake sizes and recurrence intervals at any given position along the fault, we will characterize the synthetic earthquake distribution using recurrence statistics. These can be reduced to two numbers, the mean repeat time (T_{ave}) of a certain size quake at a specific site and a coefficient of aperiodicity. The aperiodicity parameter measures the spread in the recurrence interval about T_{ave}. The spread can be deter-

mined by fitting, for example, a lognormal or Weibull function to the distribution of recurrence intervals. Nishenko and Buland (1987) and the WGCEP (1988, 1990) preferred the lognormal distribution. Ward (1992a) found Weibull functions to provide a slightly better fit to model recurrences. The values of lognormal and Weibull spreads are very close. We will use the spread, v, of a Weibull distribution.

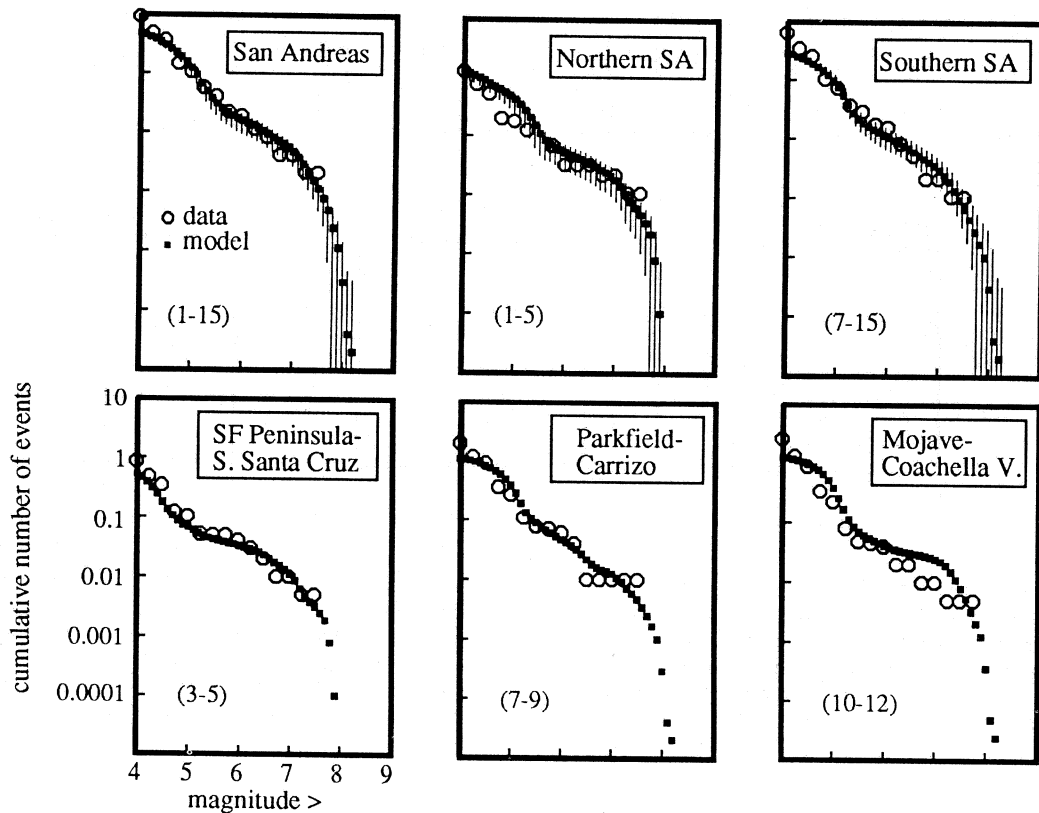The significance of the aperiodicity parameter is illustrated in fig. 7. If $v = 0$ the recur-

Fig. 6. Observed and modeled seismicity for the whole fault as well as portions of the fault. A 100 000 year run of the model reproduces seismicity for magnitudes from 4.5 up to about 8. Circles represent the observed and squares the modeled seismicity. The vertical bars on the top three model curves span one standard deviation about the mean of 500, 200 year intervals selected from the 100 000 year run. This variation compares to the uncertainty in the data that can be expected as a result of the shortness of the historical catalog. The variability in seismicity along the fault is reproduced quite well by the model.
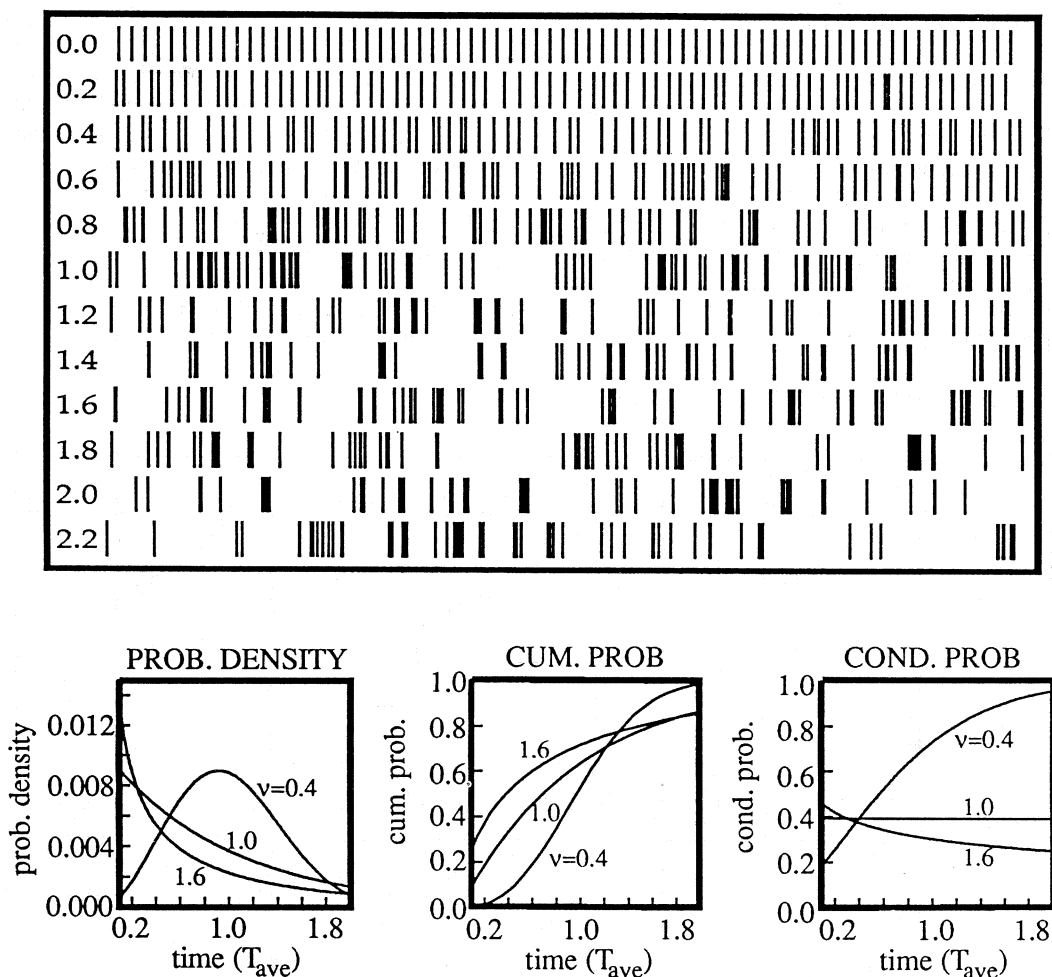
Fig. 7. Top panel shows a visualization of the effect of the aperiodicity parameter v on the recurrence of earthquakes. These 12 «bar code» lines show events drawn from a Weibull distribution of equal T_{ave} with v increasing from 0.0 to 2.2. At the bottom, Weibull probability density distributions for $v = 0.4$, 1.0 and 1.6 plus corresponding cumulative and conditional probability curves are shown. Time series with $v < 1$ and $v > 1$ are termed quasi-periodic and clustered respectively. For $v < 1$ the seismic gap concept, where probability is assumed to increase with gap time is applicable. Conversely, conditional probability decreases with gap time for $v > 1$.

rence sequence is perfectly periodic. As v gets larger, periodicity becomes more disrupted (fig. 7, top). The value of v is also related to gap time probability (fig. 7, bottom). If v is less than 1.0 probability increases with time since the last event. If v is greater than 1.0, the effect is reversed and conditional probability decreases as time increases, *i.e.* events cluster. Nishenko and Buland (1987) found that $M7$ events behave quasi-periodically with an intrinsic (lognormal) aperiodicity of 0.21. The Working Group (1988, 1990) used values

between 0.3 and 0.6. Kagan and Jackson (1991a,b) advocate clustering for events of all magnitudes, implying aperiodicity values > 1.

5.1. *Model results*

Recurrence statistics for our San Andreas fault model are listed in table IV. The bottom rows of this table give the statistics for the combined set of recurrence intervals of the whole fault. There is a clear trend of decreasing aperiodicity with increasing event magnitude. Only the largest events (M at least 7) display quasi-periodic behavior. Toward lower magnitudes, M6-6.5, clustering becomes the dominant mode of recurrence, as these events are often fore-or aftershocks. Furthermore, aperiodicity is affected by the position of a segment between other segments. For example, segments bordered by a creeping zone can behave more independently and therefore more regularly than others bordered by two strong

segments (table IV). The model recurrence behavior shows aspects of both quasi-periodic behavior (for the largest events), as was assumed by the Working Group (1988, 1990) and clustering (for the smaller events), as Kagan and Jackson (1991a,b) advocate.

5.2. *Comparison with data*

We can compare the model results with paleoseismic data for the San Andreas fault as well as a global data set of mostly historical recurrence data (Goes, submitted to *J. Geophys. Res.*, 1994).

Average recurrence times – In some places along the San Andreas fault the earthquake record has been extended considerably by paleoseismic work. At Pallett Creek, Wrightwood and Indio (PC, WW and IN, fig. 8) trenching and radioactive dating (Sieh *et al.*, 1989; Fumal *et al.*, 1993; Sieh, 1986) have resulted in a

Table IV. Recurrence statistics for the San Andreas model. Average recurrence time (T_{ave}) and aperiodicity (v) are shown per segment and as a function of magnitude.

| segment	$M \geq 6$		$M \geq 6.5$		$M \geq 7$		$M \geq 7.5$	
	T_{ave}	v	T_{ave}	v	T_{ave}	v	T_{ave}	v
1	77	1.35	85	1.24	104	1.07	229	0.51
2	71	1.62	90	1.37	109	1.16	216	0.54
3	70	1.44	77	1.32	113	0.95	352	0.53
4	39	1.39	54	1.24	105	0.95	436	0.54
5	64	1.37	77	1.16	153	0.63	608	0.74
6								
7	27	1.12	59	1.01	121	0.86	376	0.39
8	51	1.37	61	1.16	116	0.90	350	0.39
9	145	1.50	166	1.31	177	1.20	284	0.57
10	85	1.41	92	1.33	104	1.18	204	0.65
11	57	1.42	64	1.18	76	1.15	195	0.66
12	79	1.45	87	1.34	109	1.09	295	0.57
13								
14	37	1.40	53	1.15	219	0.77		
15	43	1.33	52	1.19	219	0.77		
combination	59	1.46	79	1.28	137	1.01	333	0.64
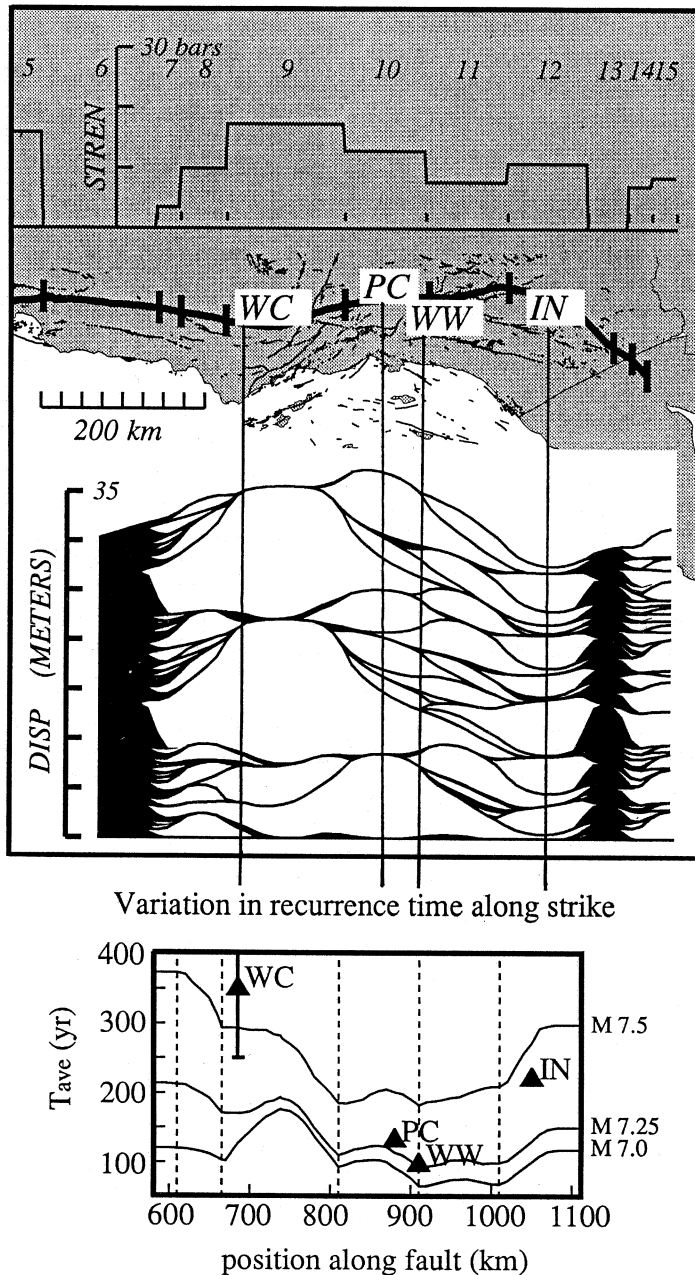
Fig. 8. The distribution of cumulative slip along the southern part of the San Andreas fault (top) indicates a large variability of recurrence modes along strike. Average recurrence times vary not only from segment to segment but also within a segment (bottom). This is very consistent with average recurrence time estimates based on paleoseismic data. Data for Wallace Creek (WC), Pallett Creek (PC) and Indio (IN) are from Sieh *et al.* (1989), for Wrightwood (WW) from Fumal *et al.* (1993).

series of 10, 5 and 4 major past events respectively. At Wallace Creek (WC, fig. 8) average recurrence intervals were obtained using stream offsets (Sieh et al., 1989). Figure 8 suggests that paleoseismic investigations at sites separated by as little as a few dozen km along strike could paint significantly different histories. For instance, at Wrightwood near the boundary of the Mojave and San Bernardino segments (WW, fig. 8) the model gives a mean repeat time of 94 years for $M \geq 7\frac{1}{4}$ quakes, whereas at Pallett Creek, 30 km to the northwest, repeat time climbs to 114 years. The observed variability in average recurrence times along the fault agrees well with the model results.

Aperiodicity – Previous work (Ward, 1992a) has shown that estimates of recurrence interval and aperiodicity will almost certainly be too low unless ten or more recurrences are spanned. Along the San Andreas fault, only the paleoseismic record at Pallett Creek (Sieh et al.,

1989) is long enough to check our estimates of irregularity. The aperiodic recurrence seen in this data set was further confirmed by Grant and Sieh (1994). Figure 9 shows the good agreement between the cumulative probability distribution based on the Pallett Creek data, for which magnitude estimates range between 7 and around 8, and cumulative model probabilities for the Mojave segment in our model. The historical record for Parkfield (Bakun and Lindh, 1985) and paleoseismic data at Wrightwood (Fumal et al., 1993) are more regular ($v = 0.33$ and $v = 0.42$ respectively) than predicted by the model, but these data sets contain only 6 and 5 events and may therefore underestimate the aperiodicity.

Aperiodicity as a function of magnitude – Recurrence data for the San Andreas are limited by the length of the historical record. To further compare our model statistics with those provided by data, we analyzed a global set of historical and paleoseismic earthquake recur-
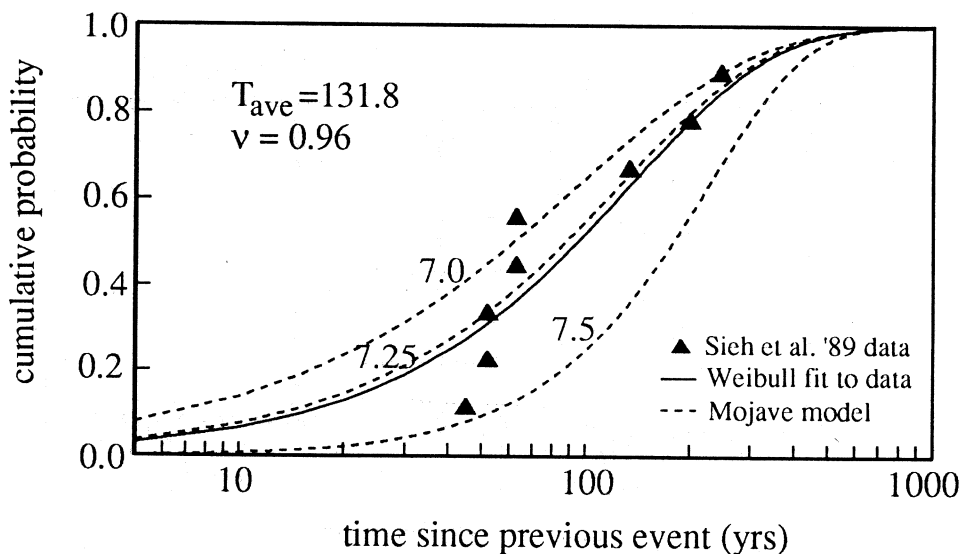

Fig. 9. There is a good agreement between the long prehistoric record for Pallett Creek (Sieh et al., 1989) and model probabilities for the Mojave segment. Symbols represent the data points from Sieh et al. (1989), with the Weibull fit (T_{ave} = 131.8 yr, v = 0.96) marked by the solid line. Dashed lines show the cumulative probabilities for the recurrence of events with magnitudes $\geq$ 7.0, 7.25 and 7.5 on our Mojave segment.

rence series of events with $M \geq 7$ from 5 major plate boundaries (Goes, submitted to *J. Geophys. Res.*, 1994). For the Middle American trench (Astiz *et al.*, 1987), the Aleutians and Alaska (Nishenko and Jacob, 1990) and Chile (Comte *et al.*, 1986; Nishenko, 1985; Kelleher, 1972) comprehensive sets of historical events are available. We also included historical data from Japan (Rikitake, 1986; Usami, 1979, 1988; Wesnousky *et al.*, 1984), and paleoseismic data for the San Andreas fault (Sieh *et al.*, 1989; Fumal *et al.*, 1993; Sieh, 1986) and Middleton Island, Alaska (Plafker, 1987). The average (lognormal) aperiodicity as a function of magnitude for this global data set is shown in fig. 10 (right). A similar aperiodicity-magnitude figure is shown for our preferred San Andreas fault model and a previous model (Ward, 1991, 1992a,b) for the Middle American trench (fig. 10, left). Both observed and predicted aperiodicity values and magnitude dependence are very similar. Although a few long series contain 8 to 10 events, most data series consist of only 3 or 4 events. The shear number of data series (50 series with 4 or more events) al-

lows us to constrain trends despite the shortness of most individual data series.

6. Probability estimates

We have shown that our model results are consistent with a variety of data ranging from segment information and seismicity distribution to paleoseismic and historical data. One way to apply the model to seismic hazard problems is by determining earthquake probabilities. The long synthetic catalog permits reliable calculation of different types of probabilities, such as gap-time probabilities for individual segments or portions of the fault, as well as non-conditional (*i.e.* average, time-independent) probabilities.

6.1. *Non-conditional probabilities*

Table V summarizes the average rate of earthquake occurrence for different rupture scenarios and magnitude ranges. These recur-
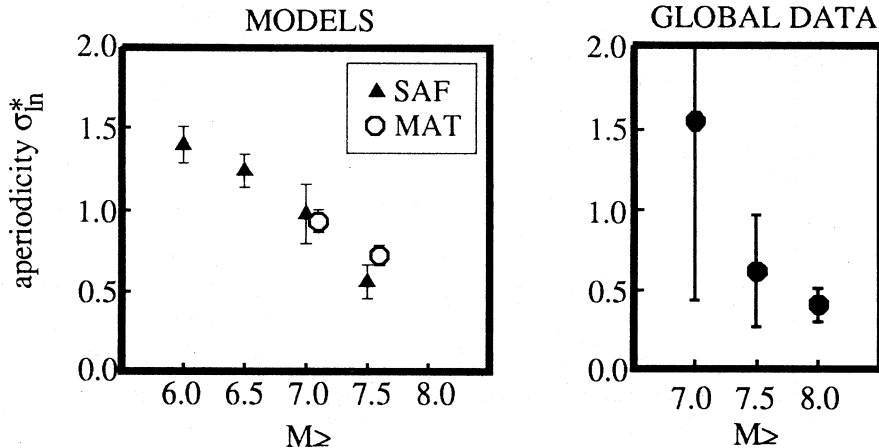

Fig. 10. Average model aperiodicities are comparable to the lognormal aperiodicity estimates (σ^{*}_{ln}) obtained from a global data analysis (Goes, submitted to *J. Geophys. Res.*, 1994). The two models for the San Andreas Fault (SAF) and Middle American Trench (MAT; Ward, 1992a) yield similar values of aperiodicity as a function of magnitude. The same trend is seen in the aperiodicity estimated from the global data set (Goes, submitted to *J. Geophys. Res.*, 1994). Symbols denote the aperiodicity averaged over all segments with its standard deviation. Only data series containing 4 or more events were included in the global data analysis.

Table V. Average model recurrence frequencies per 100 years for different rupture scenarios and magnitude ranges. These statistics allow for the calculation of the average (time-independent) probability for any given segment or rupture mode. Segment numbers correspond to those in fig. 1 and table I.

Segments broken	$M \geq 6$	$M \geq 6.5$	$M \geq 7$	$M \geq 7.5$	$M \geq 8$
1	0.473	0.387	0.196		
2	0.950	0.184	0.042		
3	0.076	0.020			
4	0.514	0.068			
5	0.005				
8	0.041	0.013			
9	0.374	0.055	0.025		
10	0.308	0.175	0.094		
11	0.533	0.295	0.132		
12	0.051				
15	0.278	0.073			
1 2	0.533	0.495	0.468	0.150	
2 3	0.112	0.078	0.016		
3 4	0.260	0.144			
4 5	0.638	0.472	0.090		
5 6	0.324	0.081			
6 7	1.610	0.025			
7 8	1.445	1.094	0.334		
8 9	0.060	0.032	0.015		
9 10	0.064	0.047	0.032		
10 11	0.318	0.300	0.267	0.016	
11 12	0.142	0.135	0.106		
12 13	0.727	0.330	0.141		
13 14	0.565	0.040			
14 15	0.225	0.205			
1 2 3	0.107	0.105	0.099	0.078	
2 3 4	0.329	0.317	0.187		
3 4 5	0.333	0.322	0.191		
4 5 6	0.183	0.176			
6 7 8	0.191	0.050			
7 8 9	0.280	0.279	0.224	0.028	
8 9 10	0.023	0.026	0.023	0.019	
9 10 11	0.097	0.095	0.094	0.059	
10 11 12	0.093	0.097	0.098	0.015	
11 12 13	0.406	0.406	0.374	0.070	
13 14 15	2.049	1.762	0.457		
1 2 3 4	0.084	0.082	0.081	0.058	
2 3 4 5	0.275	0.273	0.251	0.021	
7 8 9 10	0.115	0.115	0.113	0.089	
8 9 10 11	0.010	0.009	0.008		
9 10 11 12	0.010	0.009	0.009		
10 11 12 13	0.227	0.228	0.227	0.156	
1 2 3 4 5	0.189	0.188	0.187	0.168	
7 8 9 10 11	0.070	0.069	0.068	0.078	0.004
9 10 11 12 13	0.048	0.050	0.050	0.050	
7 8 9 10 11 12	0.036	0.036	0.034	0.033	
7 8 9 10 11 12 13	0.058	0.058	0.059	0.059	0.023

1509

rence frequencies again illustrate that each seg-
ment can break in several modes of rupture.
Furthermore, these statistics provide a time-in-
dependent estimate of the probability that a
specified segment or group of segments will
rupture. Since recurrence is quite close to Pois-

sonian ($v \approx 1$), these average values give pretty
good estimates of the probability levels at any
given time. Non-conditional probabilities can
also be used to infer whether a conditional
probability estimate is relatively high or low.
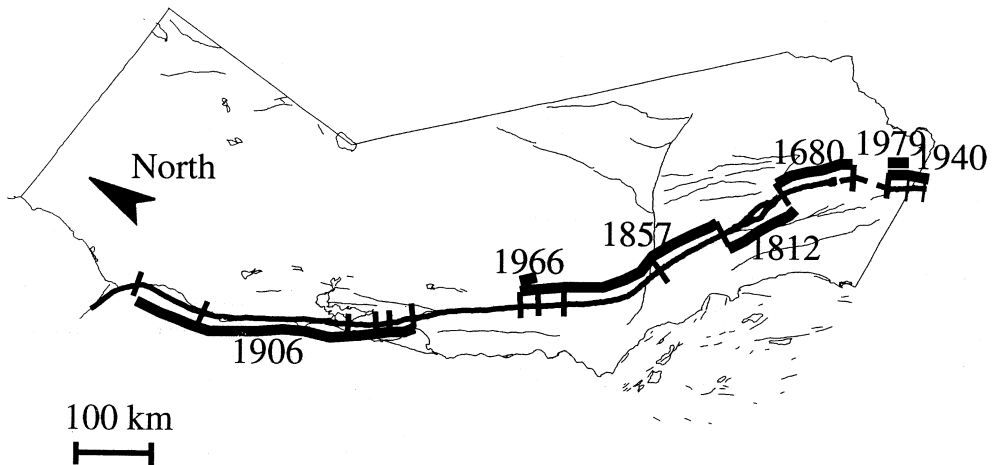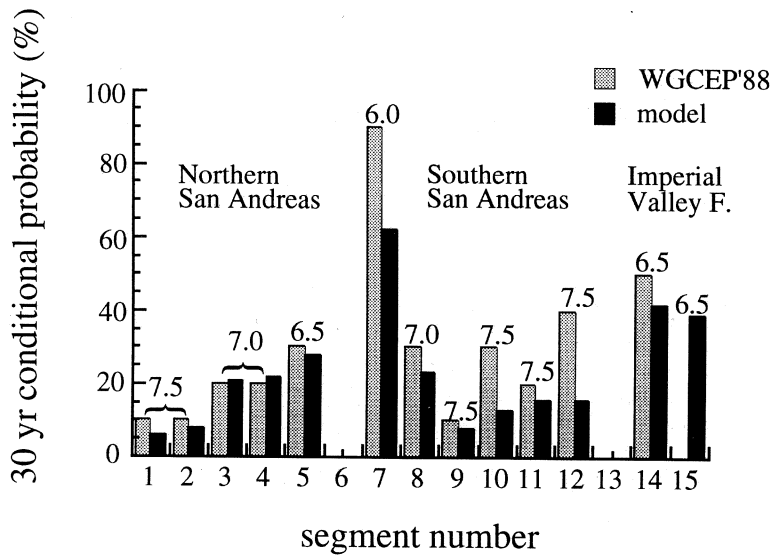For example, the non-conditional probability

Fig. 11. Comparison of model and WGCEP (1988) 30-yr gap conditional probabilities based on segment-
specific recurrence magnitude and gap time. The WGCEP (1988) assumed a much more regular recurrence for
large earthquakes than we find. This leads to their higher estimates of probability. The map displays the extent
of rupture for the earthquakes on which the probability estimates were based. Magnitudes are shown above the
bars in the diagram (top).

for an $M \geq 6$ event on the Parkfield segment in a 10 year interval is 38%. The conditional probability of recurrence of a $M \geq 6$ quake within the ten year Parkfield prediction window beginning in 1983 is 32% (versus 95% estimated by Bakun and Lindh, 1985).

6.2. *Conditional probabilities*

The Working Group (1988, 1990) combined available recurrence and slip rate data to determine conditional probability levels. Probabilities were calculated given a gap time since the last event and a magnitude of the (previous and future) event. With weaker earthquake periodicity found from our modeling, the effect of gap time recedes. This results in lower probability values than those estimated by the WG-CEP (1988, 1990) for most San Andreas segments (fig. 11). In the case of the Parkfield segment for example, the conditional probability of recurrence of a $M \geq 6$ quake within the 30 year window starting in 1988 is 69% versus more than 90% estimated by the WGCEP (1988). For the Coachella segment which has not broken in over 300 years, the 30 yr probability of failure drops to 15% from WGCEP's (1988, 1990) value of 40%. Discrepancies for other segments are not as large and depend mainly on the difference between the aperiodicity used by the WGCEP and v predicted by the model. On the Northern Imperial Valley segment our probability estimate is slightly higher than the WGCEP's. This can be attributed to the clustering of small earthquakes in our model, plus the short gap time for this segment.

Since the model intrinsically includes segment interaction, the model catalog can be used for other probability estimates, such as probabilities combined for several segments of the fault or the probability on one segment after an event on an adjacent segment. For the Mojave, San Bernardino, and Coachella segments combined, the model predicts about a one-in-three and a one-in-eight chance of a $M7+$ or $M7.5+$ quake in the next 30 years. This level of probability is about average for this part of the San Andreas (table V). We also

estimated the effect of a characteristic event (such as the $M6.9$ Loma Prieta event of 1989) on the Southern Santa Cruz Mountains segment on probability levels. It turns out that clustering of relatively small events leads to a raised probability for a $M \geq 6.5$ event on the Northern Santa Cruz Mountains segment. For events larger than $M7$ and any events on the Mid Peninsula and the Southern Santa Cruz Mountains segment itself however, probabilities remain near average level.

7. Conclusions

We believe that our synthetic seismicity model provides a useful tool to improve fault specific recurrence statistics and seismic hazard estimates. With constraints available from geological and seismological data we obtained a model that reproduces fault specific seismicity over four orders of magnitude. Furthermore, recurrence statistics based on the model agree well with paleoseismic data for the San Andreas fault, as well as with global set of historical and paleoseismic earthquake recurrence data. Segment interaction is an essential ingredient in modeling earthquake recurrence behavior. It leads to earthquake recurrence behavior varying from clustering for $M6$-6.5 events to quasi-periodic behavior for the largest ($M7.5$) events. The large aperiodicities inferred from our modeling usually imply lower gap-time probabilities than previously published for the San Andreas fault (WGCEP, 1988, 1990).

REFERENCES

ASTIZ, L., H. KANAMORI and H. EISSLER (1987): Source characteristics of earthquakes in the Michoacan seismic gap in Mexico, *Bull. Seismol. Soc. Am.*, **77**, 1326-1346.

BAKUN, W.H. and A.G. LINDH (1985): The Parkfield, California earthquake prediction experiment, *Science*, **229**, 619-624.

BEN-ZION, Y., and J.R. RICE (1993): Earthquake failure sequences along a cellular fault zone in a three-dimensional elastic solid containing asperity and non-asperity fault regions: application to Parkfield, *J. Geophys. Res.*, **98**, 14109-14131.

CHEN, Y.T. and L. KNOPOFF (1987): Simulation of earthquake sequences, *Geophys. J.R. Astron. Soc.*, **91**, 693-709.

COMTE, D., A. EISENBERG, E. LORCA, M. PARDO, L. PONCE, R. SARAGONI, S.K. SINGH and G. SUÁREZ (1986): The 1985 Central Chile earthquake: a repeat of previous great earthquakes in the region?, *Science*, **233**, 449-453.

DAVISON, F. and C. SCHOLZ (1985): Frequency-moment distribution of earthquakes in the Aleutian Arc: a test of the characteristic earthquake model, *Bull. Seismol. Soc. Am.*, **75**, 1349-1362.

ELLSWORTH, W.L. (1990): Earthquake history, 1769-1989, *U.S. Geological Survey Prof. Pap.*, **1515**, 153-187.

FUMAL, T.E., S.K. PEZZOPANE, R.J. WELDON II and D.P. SCHWARTZ (1993): A 100-year average recurrence interval for the San Andreas fault at Wrightwood, California, *Science*, **259**, 199-203.

GRANT, L.B. and K.E. SIEH (1994): Paleoseismic evidence of clustered earthquakes on the San Andreas fault in the Carrizo plain, California, *J. Geophys. Res.*, **99**, 6819-6841.

HARRIS, R.A. and R.W. SIMPSON (1992): Change in static stress on Southern California faults after the 1992 Landers earthquake, *Nature*, **360**, 251-254.

HARRIS, R.A. and S.M. DAY (1993): Dynamics of fault interaction: parallel strike-slip faults, *J. Geophys. Res.*, **98**, 4461-4472.

KAGAN, Y. and D. JACKSON (1991a): Long-term earthquake clustering, *Geophys. J. Int.*, **104**, 117-133.

KAGAN, Y. and D. JACKSON (1991b): Seismic gap hypothesis: ten years after, *J. Geophys. Res.*, **96**, 21419-21431.

KANAMORI, H. and K. MCNALLY (1982): Variable rupture mode of the subduction zone along the Ecuador-Colombia coast, *Bull. Seismol. Soc. Am.*, **72**, 1241-1254.

KELLEHER, J.A. (1972): Rupture zones of large South American earthquakes and some predictions, *J. Geophys. Res.*, **77**, 2087-2130.

KING, C. and Z. MA (1988): Migration of historical earthquakes in California, *PAGEOPH*, **127**, 627-639.

MCCANN, W.R., S.P. NISHENKO, L.R. SYKES and J. KRAUSE (1979): Seismic gaps and plate tectonics: seismic potential for major boundaries, *PAGEOPH*, **117**, 1082-1147.

NISHENKO, S.P. (1985): Seismic potential for large and great interplate earthquakes along the Chilean and Southern Peruvian margins of South America: a quantitative reappraisal, *J. Geophys. Res.*, **90**, 3589-3615.

NISHENKO, S.P. and R. BULAND (1987): A generic recurrence interval distribution for earthquake forecasting, *Bull. Seismol. Soc. Am.*, **77**, 1382-1399.

NISHENKO, S.P. and S.K. SINGH (1987): The Acapulco-Ometepec, Mexico, earthquakes of 1907-1982: evidence for a variable recurrence history, *Bull. Seismol. Soc. Am.*, **77**, 1359-1367.

NISHENKO, S.P. and K.H. JACOB (1990): Seismic potential of the Queen Charlotte-Alaska-Aleutian seismic zone, *J. Geophys. Res.*, **95**, 2511-2532.

PLAFKER, G. (1987): Application of marine-terrace data to paleoseismic studies, in *Proceedings of Conference XXXIX - Directions in Paleoseismology: U.S. Geol. Surv.*, edited by A.J. CRONE and E.M. ONDAHL, *Open-File Report*, **87-92**, 146-156.

RIKITAKE, T. (1986): Earthquake prediction in the heart of Japan, *Earthquake Pred. Res.*, **4**, 220-223.

RUNDLE, J.B. (1988a): A physical model for earthquakes 1. Fluctuations and interactions, *J. Geophys. Res.*, **93**, 6237-6254.

RUNDLE, J.B. (1988b): A physical model for earthquakes 2. Application to Southern California, *J. Geophys. Res.*, **93**, 6255-6274.

SHIMAZAKI, K. and T. NAKATA (1980): Time-predictable recurrence model for large earthquakes, *Geophys. Res. Lett.*, **7**, 279-282.

SCHWARTZ, D.P. and K.J. COPPERSMITH (1984): Fault behavior and characteristic earthquakes: examples from Wasatch and San Andreas fault zones, *J. Geophys. Res.*, **89**, 5681-5698.

SIEH, K. (1986): Slip rate across the San Andreas fault and prehistoric earthquakes at Indio, California, *EOS*, **67**, 1200.

SIEH, K., M. STUIVER and D. BRILLINGER (1989): A more precise chronology of earthquakes produced by the San Andreas fault in Southern California, *J. Geophys. Res.*, **94**, 603-623.

STEIN, R.S., G.C.P. KING and J. LIN (1992): Change in failure stress on the Southern San Andreas fault system caused by the 1992 magnitude = 7.4 Landers earthquake, *Science*, **258**, 1328-1332.

STUART, W.D. (1986): Forecast model for large and great earthquakes in Southern California, *J. Geophys. Res.*, **91**, 13771-13786.

SYKES, L.R. and S.P. NISHENKO (1984): Probabilities of occurrence of large plate rupturing earthquakes for the San Andreas, San Jacinto, and Imperial faults, California, 1983-2003, *J. Geophys. Res.*, **89**, 5905-5927.

THATCHER, W. (1990): Order and diversity in the modes of circum-Pacific earthquake recurrence, *J. Geophys. Res.*, **95**, 2609-2623.

USAMI, T. (1979): Study of historical earthquakes in Japan, *Bull. Earthq. Res. Inst.*, **54**, 399-439.

USAMI, T. (1988): Study of historical earthquakes in Japan, in *Historical seismograms and Earthquakes of the World*, edited by W.H.K. LEE, H. MEYERS and K. SHIMAZAKI, 276-288.

WARD, S.N. (1991): A synthetic seismicity model for the Middle America Trench, *J. Geophys. Res.*, **96**, 19800-19810.

WARD, S.N. (1992a): An application of synthetic seismicity calculations in earthquake statistics: The Middle America Trench, *J. Geophys. Res.*, **97**, 6675-6682.

WARD, S.N. (1992b): Computer models of seismicity: an application in long-term earthquake prediction, *Geotimes*, **37**, 19-22.

WARD, S.N. and S.D.B. GOES (1993): How regularly do earthquakes recur? A synthetic seismicity model for the San Andreas Fault, *Geophys. Res. Lett.*, **20**, 2131-2134.

WESNOUSKY, S.G. (1986): Earthquake, quarternary faults, and seismic hazard in California, *J. Geophys. Res.*, **91**, 12587-12631.

WESNOUSKY. S.G. (1994): The Gutenberg-Richter or characteristic earthquake distribution, which is it?, *Bull. Seismol. Soc. Am.*, **84**, 1940-1959.

WESNOUSKY, S.G., C.H. SCHOLZ, K. SHIMAZAKI and T. MATSUDA (1983): Earthquake frequency distribution and the mechanics of faulting, *J. Geophys. Res.*, **88**, 9331-9340.

WESNOUSKY, S.G., C.H. SCHOLZ, K. SHIMAZAKI and T. MATSUDA (1984): Integration of geological and seismological data for the analysis of seismic hazard: a case study of Japan, *Bull. Seismol. Soc. Am.*, **74**, 687-708.

WORKING GROUP ON CALIFORNIA EARTHQUAKE PROBABILITIES (WGCEP) (1988): Probabilities of large earthquakes occurring in California on the San Andreas Fault, *U.S. Geol. Surv., Open File Report*, **88-398**, pp. 62.

WORKING GROUP ON CALIFORNIA EARTHQUAKE PROBABILITIES (WGCEP) (1990): Probabilities of large earthquakes in the San Francisco Bay Region, California, *U.S. Geol. Surv. Circular*, **1053**, pp. 35.